First-principles predictions of low-energy phases of multiferroic BiFeO₃

Oswaldo Diéguez, O. E. González-Vázquez, Jacek C. Wojdeł, and Jorge Íñiguez

Institut de Ciència de Materials de Barcelona (ICMAB-CSIC), Campus UAB, E-08193 Bellaterra, Spain

We used first-principles methods to perform a systematic search for potentially stable phases of multiferroic BiFeO₃. We considered a simulation cell compatible with the atomic distortions that are most common among perovskite oxides and found a large number of local minima of the energy within 100 meV/f.u. of the ferroelectric ground state. We discuss the variety of low-symmetry structures discovered, as well as the implications of these findings as regards current experimental (e.g., on thin films displaying *supertetragonal* phases) and theoretical (on models for BiFeO₃'s structural phase transitions) work on this compound.

I. INTRODUCTION

The perovskite oxide BiFeO₃ (BFO) continues to reveal itself as one of the most intriguing materials of the day. Not only does it remain the most promising magnetoelectric multiferroic for applications at room temperature, but it also has been shown recently to display a variety of novel fundamental effects.[1] Such findings range from an increased conductivity at specific ferroelectric domain walls[2] to new structural phases in thin films[3,4] with potentially useful response properties.[5,6]

The present work originated from our ongoing research on enhancing the properties of BFO by forming solid solutions such as $BiFe_{1-x}Co_xO_3$ (Ref. 7) and $Bi_{1-x}R_xFeO_3$ with $R =$ La,Sm,Dy.[8] While investigating the chemically induced structural transitions, it became clear we needed to have a thorough and unbiased strategy to search for possible structural phases beyond those reported in the literature. Interestingly, when we applied such a scheme to BFO itself, we found plenty of low-symmetry phases that are local minima of the energy. Here we describe the lowest-energy structures that we discovered, i.e., those most likely to be observed experimentally. We discuss the origin of the large variety of distortions found in the calculations, and the possibility of capturing BFO's structural richness within simple models. Further, we comment on the implications of our findings as regards current experimental work on BFO in both bulk and thin film forms.

II. METHODOLOGY

For the simulations we used the local density approximation[9] (LDA) and generalized gradient approximation (with the Perdew-Burke-Ernzerhof [PBE (Ref. 10)] functional and its version optimized for solids [PBEsol (Ref. 11)]) to density functional theory (DFT) as implemented in the VASP package.[12] A "Hubbard-U" scheme with $U = 4$ eV was used for a better treatment of iron's $3d$ electrons;[13] the corrected DFT functionals will thus be referred to as LDA+U, PBE+U, and PBEsol+U. We used the "projector augmented wave" method to represent the ionic cores,[14] solving for the following electrons: Fe's $3p$, $3d$, and $4s$; Bi's $5d$, $6s$, and $6p$; and O's $2s$ and $2p$. (We checked that qualitatively correct results can be obtained without considering semicore electrons.) Wave functions were represented in a plane-wave basis truncated at 500 eV, and a $2 \times 2 \times 2$ k-point grid was used for integrations within the Brillouin zone (BZ)

corresponding to the 40-atom cell of Fig. 1. The calculation conditions were checked to render converged results.

We worked with the 40-atom cell depicted in Fig. 1, which is obtained by doubling the five-atom cell of the ideal perovskite structure along the three Cartesian directions, denoted by x, y, and z in the following. This cell is compatible with the structural distortions that characterize the low-symmetry phases of many perovskite oxides:[15] (1) ferroelectric (FE) patterns associated with irreducible representation Γ_4^- (symmetry labels correspond to the BZ of the five-atom cubic cell); (2) antiferroelectric (AFE) modes associated with zone-boundary q points (X-like, M-like, and R); and (3) antiferrodistortive (AFD) patterns corresponding to any combination of in-phase (M_3^+) and antiphase (R_4^+) rotations of the O₆ octahedra around the Cartesian axes. This cell is also compatible with the antiferromagnetic (AFM) spin arrangements known to be most relevant for BFO, i.e., the C-AFM and G-AFM orders sketched in Figs. 1(b) and 1(c), respectively.

To explore all these possibilities we considered a large number of starting configurations for our structural relaxations. Specifically, we considered (1) all AFD patterns consisting of either an in-phase or an antiphase rotation around each Cartesian axis (i.e., those expressible in Glazer's notation[15]); (2) various FE and AFE patterns constructed by off-centering the Bi cations; (3) cells with cubic, tetragonal, and orthorhombic shapes; (4) G- and C-AFM orders as well as a few attempts with other spin arrangements. This added up to more than 300 starting configurations. In all cases, we first ran a short molecular dynamics simulation with random initial velocities (thus breaking all symmetries), and then performed a full structural relaxation. We used the PBE+U functional for this structural search. The lowest-energy configurations obtained were confirmed to be minima by checking their stability against ionic and cell distortions.

III. RESULTS

A. Lowest-energy phases found

Our search led to a wealth of local minima with energies in a range up to 200 meV/f.u. above BFO's ground state. Table I lists the lowest-lying solutions; we show their PBE+U energy directly obtained from our structure search, as well as the energies obtained by relaxing the PBE+U structure using the PBEsol+U and LDA+U functionals.
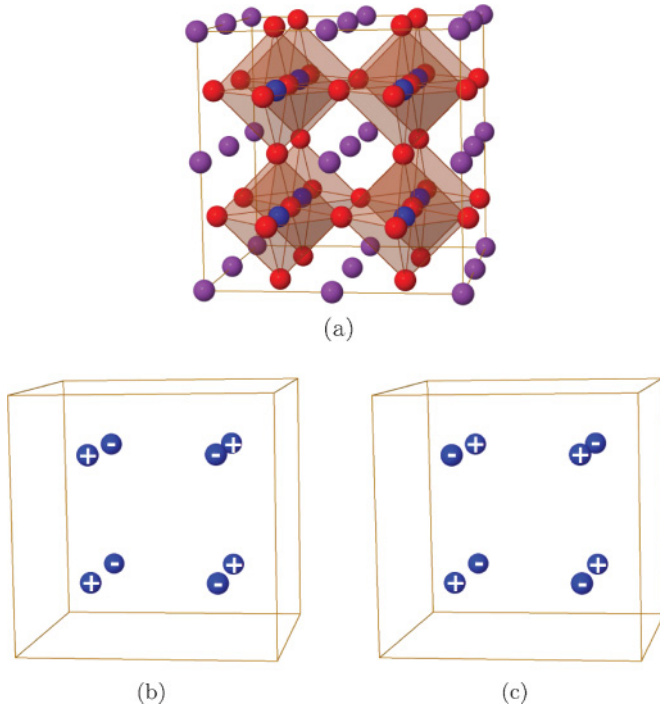
FIG. 1. (Color online) (a) 40-atom supercell of $BiFeO_3$ (extra periodic images of some O and Bi atoms have been included for easier visualization). The O atoms occupy the vertices of the octahedra plotted, which contain Fe atoms at their centers; the rest of the atoms are Bi. (b) Same cell as (a), illustrating a C-AFM arrangement of Fe atom spins. (c) Same as (b), but with a G-AFM spin arrangement. All the phases considered in this work have unit cells that are distortions of the one depicted here.

Note that the energy differences between phases are strongly dependent on the DFT functional; we will address this issue below. Table I also includes a short description of the phases found, which we label by their atomic space group and type of AFM order (e.g., $R3c$-G for the ground state); the complete structural information and computed polarization values[16] are given in Tables II and III. Let us note that our work with BFO and other compounds confirms that the PBEsol functional is more accurate than the PBE and LDA approaches for predicting the atomic structure of individual phases.[11] Thus, the crystallographic data reported here correspond to (PBEsol+U)-relaxed structures. Finally, Fig. 2 shows sketches of the structures obtained, and the most relevant distortion modes are depicted in Fig. 3.

All the functionals correctly predict the $R3c$ phase with G-AFM spin order as the ground state of BFO. This phase displays a spontaneous polarization along the [111] Cartesian direction and antiphase O_6 rotations around the same axis ($a^-a^-a^-$ in Glazer's notation).

We also found two orthorhombic phases that are similar to $R3c$-G in that they involve a relatively small distortion of the ideal cubic cell and favor the G-AFM order: $Pnma$-G and $Pna2_1$-G.

The $Pnma$-G structure is paraelectric (PE). As shown in Table I, it is characterized by an O_6 rotation pattern ($a^-a^-b^+$) that involves anti-phase rotations around [110] and in-phase rotations around [001]. This phase is the ground state of many perovskites, $LaFeO_3$ being the most relevant one for the current discussion. Interestingly, BFO's $Pnma$-G phase can be aptly described as AFE, because the Bi cations present large antipolar displacements in the (001) plane (associated with the X_5^+ mode of Table I and Fig. 3); the computed off-centering of the Bi cations is about 0.3 Å. (Such an AFE

TABLE I. Energies and distortions of the most stable energy minima found (seven top phases), as well as a few saddle points (six bottom phases) included for reference. Columns 2–4: Energies obtained with different DFT functionals. Note $Pna2_1$-G goes to $Pnma$-G when relaxed with PBEsol+U and LDA+U. Columns 5–8: Distortions from the ideal cubic perovskite structure ($Pm\bar{3}m$) that characterize the phases. In all cases the FE and AFD modes fully determine the symmetry breaking. A generic $[x,y,z]$ FE (AFD) distortion involves displacements (O_6 rotations) along (around) the x, y, and z Cartesian axes. We indicate the dominant FE and AFD distortions in bold. Column 8 includes other modes with a significant contribution (at least 10% of the largest one). The mode analysis was done with the ISODISPLACE software (Ref. 66); note that q points indicated in symmetry labels constitute default choices and do not always correspond to the actual distortion modulation (e.g., the X_5^+ and X_5^- AFE modes in the table are actually modulated along the z direction).

| Phase | $\Delta E = E - E(R3c\text{-G})$ (meV/f.u.) | | | Structural distortions | | | |
	PBE+U	PBEsol+U	LDA+U	Γ_4^- (FE)	R_4^+ (AFD)	M_3^+ (AFD)	Additional distortions
Pc-C	19	106	134	$[x,x,\mathbf{z}]$	–	$[0,0,z]$	AFE (M_5^-), O_6-dist. (Γ_5^-), $c/a = 1.27$
Cm-C	12	103	132	$[0,y,\mathbf{z}]$	–	$[0,y,0]$	O_6-dist. (Γ_5^-), $c/a = 1.27$
$Pna2_1$-C	14	99	127	$[0,0,\mathbf{z}]$	$[x,x,0]$	$[0,0,z \approx 0]$	AFE (X_5^+,X_5^-,R_5^+), $c/a = 1.26$
Cc-C	10	96	125	$[x,x,\mathbf{z}]$	$[x,x,z \approx 0]$	–	AFE (R_5^+), O_6-dist. (Γ_5^-), $c/a = 1.25$
$Pnma$-G	60	27	14	–	$[\mathbf{x},\mathbf{x},0]$	$[0,0,z]$	AFE (X_5^+,R_5^+)
$Pna2_1$-G	47	–	–	$[0,0,z]$	$[\mathbf{x},\mathbf{x},0]$	$[0,0,z]$	AFE (X_5^+,X_5^-)
$R3c$-G	0	0	0	$[\mathbf{x},\mathbf{x},\mathbf{x}]$	$[\mathbf{x},\mathbf{x},\mathbf{x}]$	–	–
$P4mm$-C	82	140	152	$[0,0,z]$	–	–	$c/a = 1.28$
$R3m$-G	136	169	191	$[\mathbf{x},\mathbf{x},\mathbf{x}]$	–	–	–
$Amm2$-G	175	203	213	$[\mathbf{x},\mathbf{x},0]$	–	–	–
$R\bar{3}c$-G	272	230	209	–	$[\mathbf{x},\mathbf{x},\mathbf{x}]$	–	–
$I4/mcm$-G	430	372	344	–	$[0,0,\mathbf{z}]$	–	–
$Pm\bar{3}m$-G	981	906	870	–	–	–	–

TABLE II. Computed PBEsol+U lattice parameters (corresponding to the 40-atom cell of Fig. 1) and polarization values for the six stable phases of BFO listed in Table I. The polarization direction is given in a Cartesian reference that corresponds almost exactly with the 40-atom cell vectors. For comparison, we also include the result for the $P4mm$-C structure.

Phase	Lattice parameters						Polarization	
	a (Å)	b (Å)	c (Å)	α (deg)	β (deg)	γ (deg)	Magnitude (C/m^2)	Direction
Pc-C	7.500	7.500	9.489	88.1	88.1	89.7	1.20	(0.29, 0.29, 0.92)
Cm-C	7.380	7.608	9.533	86.6	90.0	90.0	1.50	(0.00, 0.30, 0.95)
$Pna2_1$-C	7.515	7.515	9.452	90.0	90.0	90.0	1.39	(0.00, 0.00, 1.00)
Cc-C	7.527	7.527	9.444	88.0	88.0	90.0	1.45	(0.23, 0.23, 0.94)
$Pnma$-G	7.830	7.830	7.770	90.0	90.0	87.6	0	–
$R3c$-G	7.893	7.893	7.893	89.5	89.5	89.5	0.91	(0.58, 0.58, 0.58)
$P4mm$-C	7.414	7.414	9.526	90.0	90.0	90.0	1.52	(0.00, 0.00, 1.00)

pattern is allowed by symmetry in LaFeO$_3$ too; in that case we obtain La off-centers by about 0.2 Å.)

The $Pna2_1$-G phase is similar to $Pnma$-G, but with an additional FE distortion along the axis of the in-phase rotations. As compared with that of $Pnma$-G, the 40-atom cell of the $Pna2_1$-G phase is elongated along the polarization direction; this reflects the usual coupling between the FE distortion and strain observed in perovskite oxides.

Regarding magnetism, the $R3c$-G, $Pnma$-G, and $Pna2_1$-G phases display strong AFM exchange couplings between neighboring Fe ions, as evidenced by a large energy splitting of more than 200 meV/f.u. between the G-AFM and ferromagnetic (FM) configurations. This is consistent with the high magnetic ordering temperature observed in bulk BFO.

In addition, we found a number of phases that involve a large stretching of the ideal cubic cell along the z direction, with c/a aspect ratios approaching 1.3. In the following we

will generically refer to such structures as *supertetragonal* or T phases. They all favor the C-AFM order (see Fig. 1), the parallel spin alignment occurring along the stretched lattice vector. The magnetic interactions along z are weak, as evidenced by an energy splitting of about 5 meV/f.u. between the C- and G-AFM orders; accordingly, the ordering temperatures will be relatively low. Three of these phases are monoclinic (Cc-C, Cm-C, and Pc-C) and one is orthorhombic ($Pna2_1$-C); all of them are ferroelectric with a very large polarization component along [001] (see computed values in Table II).

More specifically, the Cc-C phase presents a polarization in the (1$\bar{1}$0) plane, as well as relatively small AFD distortions. This type of monoclinic phase is usually termed M_A;[17] a similar phase has been studied theoretically in connection with the supertetragonal structures observed experimentally in BFO films.[3,5,6,18]

(a) Pc-C

(b) Cm-C

(c) $Pna2_1$-C

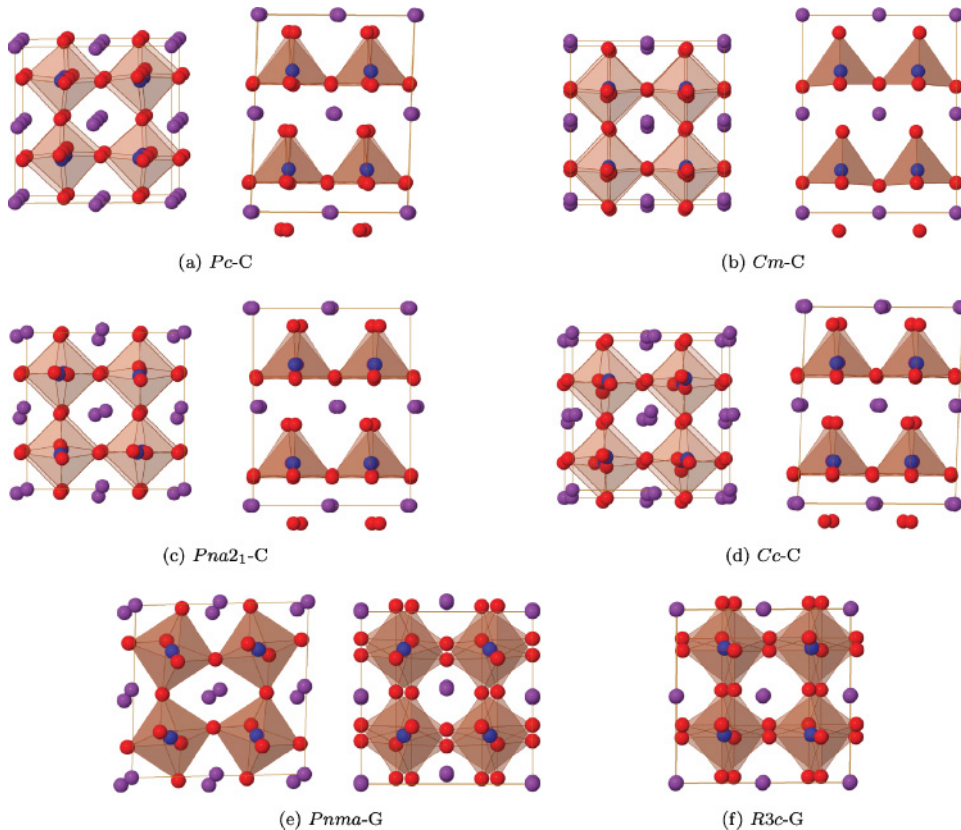(d) Cc-C

(e) $Pnma$-G

(f) $R3c$-G

FIG. 2. (Color online) Energy minimum configurations obtained. (a)–(d) C-AFM supertetragonal phases; in the left (right) image the c axis is perpendicular (parallel) to the page. (e)–(f) G-AFM phases; two pseudocubic axes are equivalent in (e), with the left (right) figure having the nonequivalent axis perpendicular (parallel) to the page; the three pseudocubic axis are equivalent in (f). The atomic species can be identified as in Fig. 1.

TABLE III. Energy minima structures of Table I as obtained from PBEsol+U calculations. In the case of the $Pna2_1$-G phase, the PBE+U result is given (see text).

Pc-C (unique axis b)		$a = 7.291$ Å	$b = 5.291$ Å $\alpha = \gamma = 90°$	$c = 5.315$ Å $\beta = 139.46°$
Atom	Wyc.	x	y	z
Bi	2a	0.8692	0.2649	0.4158
Fe	2a	0.4372	0.2467	0.4361
O	2a	0.0471	0.7150	0.5161
O	2a	0.5781	0.5084	0.3342
O	2a	0.5609	0.0152	0.2979

Cm-C (unique axis b)		$a = 9.534$ Å	$b = 7.380$ Å $\alpha = \gamma = 90°$	$c = 3.804$ Å $\beta = 86.60°$
Atom	Wyc.	x	y	z
Bi	2a	0.4948	0	0.9617
Bi	2a	0.9959	0	0.9418
Fe	4b	0.2810	0.2482	0.5184
O	2a	0.3590	0	0.5151
O	2a	0.8446	0	0.5261
O	4b	0.0864	0.2388	0.5689
O	4b	0.3449	0.2443	0.0153

$Pna2_1$-C		$a = 5.314$ Å	$b = 5.314$ Å $\alpha = \beta = \gamma = 90°$	$c = 9.452$ Å
Atom	Wyc.	x	y	z
Bi	4a	0.5451	0.4799	0.4590
Fe	4a	0.0195	0.5127	0.2448
O	4a	0.0357	0.5476	0.0493
O	4a	0.2669	0.7524	0.3170
O	4a	0.2633	0.2491	0.3058

Cc-C (unique axis b)		$a = 10.604$ Å	$b = 5.322$ Å $\alpha = \gamma = 90°$	$c = 5.323$ Å $\beta = 62.80°$
Atom	Wyc.	x	y	z
Bi	4a	0.4829	0.7707	0.1102
Fe	4a	0.2689	0.2630	0.2799
O	4a	0.0727	0.2986	0.4448
O	4a	0.3290	0.9986	0.4671
O	4a	0.3405	0.5032	0.4593

$Pnma$-G		$a = 5.650$ Å	$b = 7.770$ Å $\alpha = \beta = \gamma = 90°$	$c = 5.421$ Å
Atom	Wyc.	x	y	z
Bi	4c	0.0523	1/4	0.0100
Fe	4b	0	0	1/2
O	4c	0.9722	1/4	0.5946
O	8d	0.2998	0.0461	0.3037

$R3c$-G		$a = b = 5.559$ Å	$\alpha = \beta = 90° \; \gamma = 120°$	$c = 13.782$ Å
Atom	Wyc.	x	y	z
Bi	6a	0	0	0.0000
Fe	6a	0	0	0.7236
O	18b	0.3156	0.2294	0.1238

TABLE III. (*Continued*)

$Pna2_1$-G (PBE+U)		$a = 5.702$ Å	$b = 5.507$ Å $\alpha = \beta = \gamma = 90°$	$c = 8.036$ Å
Atom	Wyc.	x	y	z
Bi	4a	0.4435	0.0016	0.2194
Fe	4a	0.5015	0.5007	0.4943
O	4a	0.2137	0.7074	0.0519
O	4a	0.1848	0.6876	0.4796
O	4a	0.5302	0.4171	0.2532

The Pc-C phase is very similar to Cc-C as regards the polar distortion (thus, it is also M_A), but it displays a different O_6-rotation pattern.

The Cm-C phase displays a polarization in the (100) plane, and the cell is significantly distorted in the xy plane; such a monoclinic phase is termed M_C.
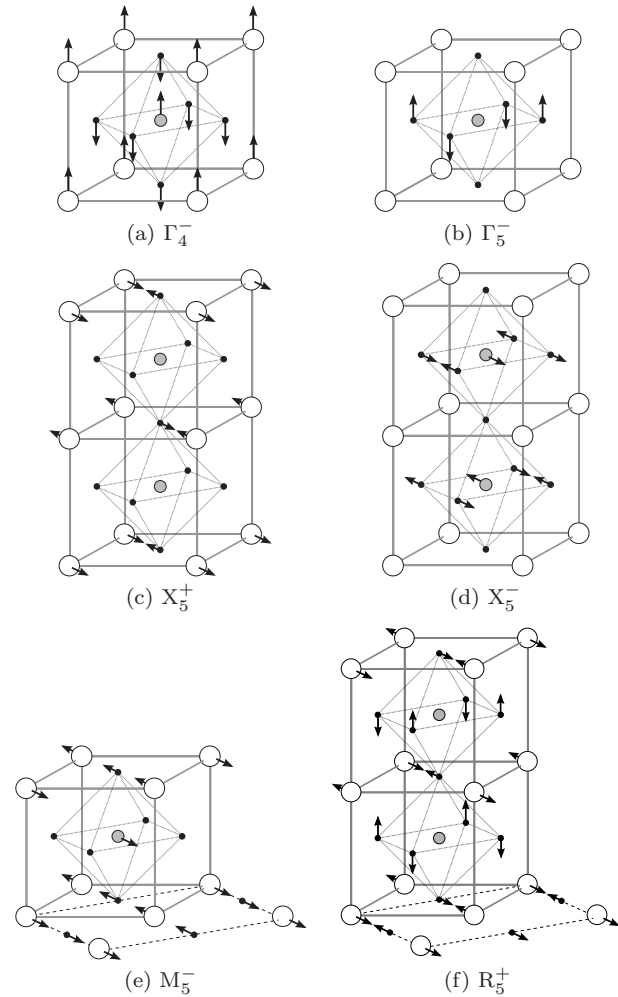

FIG. 3. Illustration of atomic displacements for different symmetry modes of BFO: (a) soft FE mode; (b)–(f) secondary modes mentioned in Table I. Only displacement directions, not magnitudes, are indicated; for the (a) case, the (PBEsol+U)-computed atomic displacements are quoted in the caption of Fig. 7. White, gray, and black circles represent Bi, Fe, and O atoms, respectively.

The $Pna2_1$-C phase is very similar to the $Pna2_1$-G structure discussed above, the stretching of the cell and development of polarization coinciding with the axis of the in-phase rotations.

Note that all these T phases can be viewed as distorted versions of the ideal supertetragonal $P4mm$-C structure listed in Table I. Interestingly, we found that this $P4mm$-C phase, which is the ground state of $BiCoO_3$,[7] is a saddle point in BFO's energy landscape.

Our results thus reveal an intricate energy landscape, especially regarding structures with a large c/a ratio. In this sense, it is interesting to note that some of the phases reported here are small distortions of higher-symmetry structures. For example, the Cm-C phase can be shown to be a Pm-C structure distorted by the M_3^+-$[0,y,0]$ mode listed in Table I; by moving from the Pm-C saddle point to the Cm-C minimum, BFO gains about 1 meV/f.u. Similarly, the reported Pc-C phase is connected with a higher-symmetry Cm-C structure *via* a M_3^+-$[0,0,z]$ distortion.[19] Given BFO's manifest complexity, we tend to view the phases of Table I as a probably incomplete list, just indicative of the rich variety of stable structures that this compound can present.

Finally, let us stress that we explicitly checked that all the above phases are local minima of the energy, a fact that is remarkable since some of them (e.g., the pairs formed by $Pnma$-G and $Pna2_1$-G, or Cc-C and Pc-C) are rather close structurally. It is also interesting to note that monoclinic phases with such small primitive cells may be energy minima by themselves, i.e., without the need of any stabilizing (electric, stress) fields. Note that, to the best of our knowledge, monoclinic phases in bulk perovskite oxides tend to be associated with complex solid solutions or large unit cells. Examples of the former are the monoclinic M_A phase that occurs in the prototype piezoelectric $PbZr_{1-x}Ti_xO_3$,[20] and the monoclinic M_C phase of relaxor $PbZn_{1/3}Nb_{2/3}O_3$-$PbTiO_3$.[21] Examples of the latter occur in $BiMnO_3$ and $BiScO_3$; see the discussion in Ref. 22. It was thus unexpected to discover that bulk BFO presents such a collection of *simple* low-symmetry minima of the energy.

B. Energy differences between phases

The relative stability of the phases discussed above is quantified by the energy differences between them. Disturbingly, Table I shows that such energy differences are strongly dependent on the DFT functional used to compute them. By switching functional we obtained changes in relative stability—e.g., $Pnma$-G is more stable than the T phases according to PBEsol+U and LDA+U, but less stable according to PBE+U—and even the loss of stability of one phase-e.g., the $Pna2_1$-G phase is stable for PBE+U, but the relaxation of this structure with PBEsol+U and LDA+U leads to the $Pnma$-G solution. Thus, we have to ask ourselves: Does any one of these functionals provide an accurate picture of the relative stability of BFO's phases? Noting that PBEsol is generally more accurate regarding the structural description of individual phases, can we just rely on the PBEsol+U results?

One would like to address this issue by resorting to a higher-level first-principles theory. However, performing quantum Monte Carlo calculations, which are the reference for accuracy
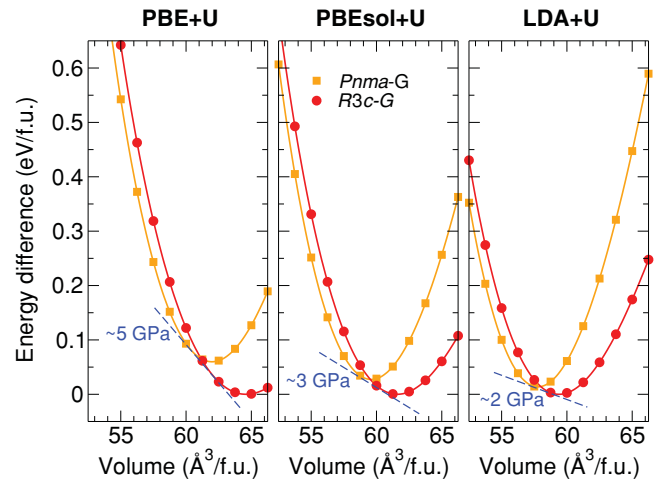

FIG. 4. (Color online) Energy versus volume curves for the most stable phases of BFO. The labels at the top indicate the DFT functional used. The transition pressures mentioned in the text were obtained by computing the slope of the common tangent of the $R3c$-G and $Pnma$-G curves.

in this context, is well beyond the scope of this work. Simpler schemes like the so-called hybrid functionals, which are usually considered to be more accurate than DFT for insulators like BFO, are not well tested for quantifying relative stabilities in cases like this one. Moreover, structural predictions with hybrids have been shown to depend strongly on the underlying generalized gradient approximation,[23] which invalidates them for the present purposes.

Nevertheless, we were able to make a couple of meaningful comparisons with experiment. First, we studied the transition between the $R3c$-G and $Pnma$-G phases that is known to occur under hydrostatic pressure.[24] We obtained (see Fig. 4) transition pressures of about 2 GPa for LDA+U, 3 GPa for PBEsol+U, and 5 GPa for PBE+U. Room-temperature experiments by Haumont *et al.*[22] showed that at 3.5 GPa the $R3c$-G phase transforms into a monoclinic $C2/m$ structure with a large cell (made of 12 formula units), and that a second transition at 10 GPa leads to the $Pnma$-G phase. These results suggest that the $R3c$-G and $Pnma$-G phases invert their relative stability at a pressure between 3.5 and 10 GPa, a bracket that can be shifted to 5–14 GPa if the transition lines are extrapolated to 0 K.[1] Thus, this comparison seems to indicate that the PBE+U is the most accurate theory for relative stability calculations, and that the LDA+U should not be used for these purposes. We have reached similar conclusions in our work with $Bi_{1-x}La_xFeO_3$ solid solutions;[25] in that case, the LDA+U calculation predicts a $R3c$-to-$Pnma$ transition for a La content that is clearly too small to be compatible with the experiments.

Second, we computed the relative stabilities of these phases as a function of an epitaxial strain corresponding to a square substrate in the (001) plane, so as to determine the lattice mismatch needed to stabilize the large-(c/a) structures.[26] As shown in Fig. 5, we obtained strain values of -2.3%, -4.0%, and -4.5% for PBE+U, PBEsol+U, and LDA+U, respectively. Experimentally it is known that a BFO-(001) thin film grown on $SrTiO_3$ (-1.5% misfit strain) displays a
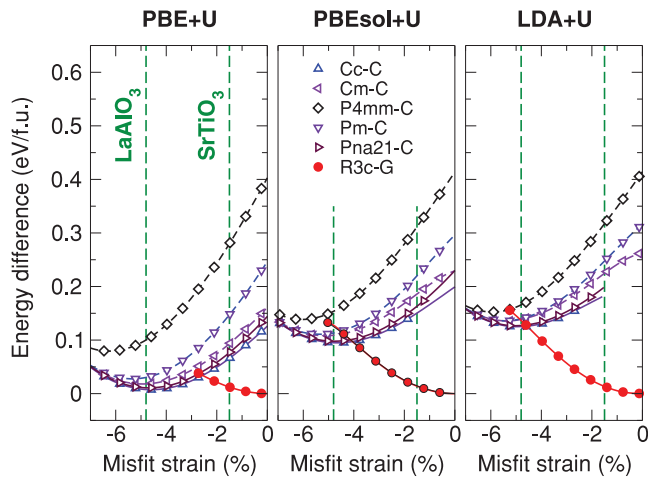
FIG. 5. (Color online) Energy of various BFO phases as a function of the misfit (epitaxial) strain corresponding to a square (001)-oriented substrate. The labels at the top indicate the DFT functional used. Note that the $R3c$-G phase reduces its symmetry to Cc-G in these epitaxial conditions.

monoclinic structure that is an epitaxially distorted version of the $R3c$ phase (such a phase is believed to be monoclinic M_A with the Cc space group[27]); we will denote this phase by R in the following. In contrast, when LaAlO$_3$ substrates (-4.8% misfit strain) are used, a supertetragonal T phase whose symmetry remains unclear,[3] or a coexistence of the R and T phases,[5] has been observed. These results suggest that the energies of the R and T phases cross at an epitaxial compression close to -4.8%. Hence, according to this criterion, and assuming that our large-(c/a) phases are good candidates to be the observed T phase, the PBE+U curves would be the least reliable ones. We have reached similar conclusions in our work with BiFe$_{1-x}$Co$_x$O$_3$ solid solutions,[28] where PBE+U predicts an R-to-T transition for a Co content that is too small to be compatible with experiment. Further, these observations seem consistent with a well-known failure of the PBE approximation: it tends to render too large tetragonal distortions in ferroelectric perovskites.[23,29]

In conclusion, while the PBE+U and LDA+U approaches seem to be rather accurate in some cases, they also render clearly wrong predictions in others. In this respect, PBEsol+U seems to be a reasonable compromise, as it constitutes the overall most accurate DFT theory available to us. Nevertheless, because PBE+U performs well as regards the relative stability of the $R3c$-G and $Pnma$-G phases, we believe that the PBE+U prediction of the new ferroelectric phase $Pna2_1$-G, structurally very similar to $Pnma$-G, deserves some attention. Finally, let us note that the choice of U also has an effect on the energy differences of Table I. Yet, for U values in the 3–5 eV range, such effects are small as compared with the ones we have discussed.

IV. DISCUSSION

Our results have direct implications for current experimental work on the structural characterization and phase transitions of BFO, especially regarding the epitaxially compressed films in which supertetragonal phases were discovered. Further,

they also provide us with information that is relevant to the effective modeling of BFO's structural transitions, at both the macroscopic (Landau-type theories) and atomistic (effective Hamiltonians) levels. In the following we discuss all these aspects. To conclude this section, we comment on Bi's ability to form very different and stable *coordination complexes* with oxygen, as this seems to be the factor responsible for the observed structural richness of BFO.

A. Implications for experimental work

1. Supertetragonal *phases in BiFeO$_3$ films*

The recent works by Béa *et al.*[3] and Zeches *et al.*[5] have shown that it is possible to obtain a novel phase of BFO if thin films are grown on strongly compressive substrates like LaAlO$_3$-(001). Experimentally, this T phase presents a very large c/a ratio of about 1.23, and an out-of-plane polarization $P_z \approx 0.8$ C/m^2. First-principles studies[5,6,18] have identified the T phase with a monoclinic Cc structure for which LDA+U calculations predict $c/a \approx 1.23$ and $P_z \approx 1.5$ C/m^2. Thus, there is a large quantitative discrepancy between theory and experiment as regards the value of P_z, which suggests that the identification of the simulated and experimental phases may be incorrect.

Our present results show that there are many possible T phases—e.g., the low-energy Pc-C, Cm-C, $Pna2_1$-C, and Cc-C structures that we found—that might correspond to the one experimentally realized in the BFO films. Indeed, as shown in Fig. 5, all our large-(c/a) phases are essentially degenerate in energy for values of the epitaxial strain corresponding to a LaAlO$_3$ substrate. Moreover, at the PBEsol+U level—which we have adopted as the DFT flavor of choice for BFO—all these phases have their energy minimum at a misfit strain of about -4.8%, implying that any of them can form a stable BFO film under such epitaxial conditions.

Because our T phases are an almost perfect epitaxial match with the LaAlO$_3$ substrate, the structural and polarization data in Tables II and III can be compared with the experimental results directly. Most remarkably, our results show that phases with very similar c/a ratios can display rather different polarization values. Indeed, the Pc-C phase (with a c/a of 1.27) presents $P_z \approx 1.1$ C/m^2, while the Cm-C and $Pna2_1$-C phases (with c/a's of 1.26 and 1.25, respectively) present $P_z \approx 1.4$ C/m^2. Hence, our Pc-C structure seems to be the best candidate to represent the T phase realized in the BFO films investigated experimentally; the quantitative disagreement between the measured and predicted P_z's would be below 40%, a clear improvement upon the previously reported 90% difference.

Let us also note that, because our T phases are so close in energy, the question of which one is realized experimentally may depend on subtle details not considered in this work. Thus, for example, two of these phases (Pc-C and Cm-C) present no *tilts* (i.e., rotations around the [100] and [010] axes) of the O$_6$ octahedra, which may make them preferable if the BFO films are grown on (001) substrates that clamp such distortions strongly. Similarly, a rectangular substrate might favor the Cm-C phase, whose cell tends to distort in the xy plane, etc.

Finally, we have very recently become aware of new results[30–32] showing that both M_C and M_A monoclinic phases with large-(c/a) ratios can be realized in epitaxially compressed BFO-(001) films. Such findings further support the physical relevance of the present study.

2. *Structural transitions in bulk BiFeO₃*

Our calculations were restricted to the limit of low temperatures, and do not allow for a conclusive discussion of temperature-driven effects and transitions in BFO.[33,34] Nevertheless, a few comments can be made based on the obtained (large) energy differences between some relevant phases. Indeed, our results seem consistent with experiments[1,35,36] showing that, as a function of increasing temperature, BFO's ferroelectric $R3c$ phase transforms into an orthorhombic $Pnma$ structure at $T \approx 1100$ K, to then become cubic $Pm\bar{3}m$ at $T \approx 1200$ K. More specifically, the PBEsol+U results of Table I show that the $R3c$-G and $Pnma$-G minima are very close in energy and constitute strong instabilities of the prototype $Pm\bar{3}m$ structure, which lies about 900 meV/f.u. above them, as consistent with the fact that BFO's cubic phase can be observed only at very high temperatures. Moreover, $R3c$-G and $Pnma$-G constitute BFO's most stable phases, with a large margin over other structures (e.g., the ferroelectric $R3m$-G and $Amm2$-G, or paraelectric $R\bar{3}c$-G and $I4/mcm$-G, listed in Table I) that are common among perovskite oxides. Hence, our results seem incompatible with the $R3c \rightarrow I4/mcm \rightarrow Pm\bar{3}m$ transition sequence obtained by Kornev *et al.*[37] from Monte Carlo simulations of first-principles-derived effective Hamiltonians; we found that the $I4/mcm$ structure has a relatively high energy and is thus unlikely to occur instead of $Pnma$.

As regards pressure-driven transitions, our results confirm that under compression BFO's $R3c$-G phase loses stability in favor of the $Pnma$-G structure.[22,38] Additionally, it is worth noting that, at the PBE+U level, we found a $Pna2_1$-G phase (see Table I) whose stability is also favored by compression and which nearly becomes the ground state in the pressure range in which $R3c$-G and $Pnma$-G revert their relative stability (results not shown here). Given that PBE+U seems the most accurate DFT flavor for the description of these pressure-induced transformations (see Sec. III B), it seems wise to bear in mind the possibility that such a $Pna2_1$-G structure might occur, especially considering that the nature of the phase intermediate between $R3c$-G and $Pnma$-G remains unclear.[22]

B. Implications for modeling work

Our results clearly demonstrate that, in spite of its apparent simplicity, BiFeO₃ is extraordinarily complex from the structural point of view. In the following sections we will *quantify* such a complexity, adopting the perspective of someone who is interested in determining the simplest possible model, either macroscopic or atomistic, that captures accurately BFO's structural diversity. Our analysis shows that BFO is much more challenging to model than *traditional* ferroelectric perovskites like BaTiO₃, PbTiO₃, or even PbZr$_{1-x}$Ti$_x$O₃.

1. *Primary and secondary distortions in BiFeO₃*

By analyzing the BFO phases described in Table I, it is possible to identify three primary distortion types (or primary order parameters) whose occurrence can explain all the symmetry reductions of interest and which must be considered in any theory of BFO's structural phase transitions: A polar distortion that can in principle be oriented along any spatial direction (Γ_4^- symmetry), and in-phase (M_3^+) and antiphase (R_4^+) O₆ rotations around the three Cartesian axes. The atomic displacements associated with the two AFD order parameters (i.e., the oxygen-octahedra rotations) are uniquely defined by symmetry; hence, these modes are trivial in this sense. In contrast, the polar distortions are not determined by symmetry: any combination of Γ_4^--like displacements of the Bi, Fe, and O sublattices is in principle valid. Following the usual first-principles approach to *simple* ferroelectric perovskites like BaTiO₃ or PbTiO₃,[39] one would determine the specific atomic displacements that define the FE order parameter by computing the unstable (soft) polar mode of the cubic phase of the compound; the result thus obtained for BFO is depicted in Fig. 3(a). In materials like BaTiO₃, such a soft mode captures very accurately the atomic distortions associated to the relevant FE phases, e.g., tetragonal $P4mm$ and rhombohedral $R3m$. It is not obvious that the same will be true for BFO, where we would like to describe *simultaneously* supertetragonal phases, which imply a very large distortion of the cubic cell, and the rhombohedral ground state, where the polar distortion coexists with very large O₆ rotations. Interestingly, we were able to demonstrate that the traditional approach works well for BFO: We performed a mode-by-mode decomposition of the atomic distortions connecting the prototype $Pm\bar{3}m$-G phase with the $P4mm$-C (as representative of our large-(c/a) phases) and $R3c$-G structures, and checked that the Γ_4^--like component is captured very accurately by the soft FE mode of the cubic phase (to within 93% for $P4mm$-C and 99% for $R3c$-G). We can thus conclude that it is possible to describe *all* the FE phases of BFO with relatively simple theories that include only one polar mode.

The three primary order parameters described above are clearly the driving force for the structural transitions in BFO. For a given phase of the material, the occurrence of a particular combination of such primary distortions involves a specific breaking of the $Pm\bar{3}m$ symmetry of the cubic perovskite structure, which in turn results in the *activation* of secondary order parameters that become allowed in the low-symmetry phase. The most significant secondary distortions that we found in our BFO's phases are listed in the last column of Table I and sketched in Fig. 3. There is a considerable number of such secondary modes; the ones involving the largest atomic displacements can be easily grouped in two categories: AFE patterns [see (c) to (f) modes in Fig. 3] and twisting modes of the O₆ octahedra [(b) in Fig. 3]. In this sense, BFO is very different from ferroelectrics like BaTiO₃ or PbTiO₃, where the relevant FE phases do not present any secondary modes (note the absence of additional distortions for the $P4mm$, $Amm2$, and $R3m$ symmetries listed in Table I, which are the relevant ones for BaTiO₃ and PbTiO₃). One thus needs to wonder: How important are these secondary distortions? Do they play a role in determining the energetics and relative stability of BFO's phases, or can they be ignored in an effective theory of BFO's structural phase transitions?[40]

We quantified the importance of the secondary modes in the following approximate manner: We considered the PBEsol+U equilibrium structures of all the relevant phases, artificially set to zero the secondary atomic distortions, and computed the energy of the modified structures. The obtained energy increments with respect to the actual equilibrium phases are very significant: they range from tens of meV/f.u. for the monoclinic (Pc-C, Cm-C, and Cc-C) phases to more than a hundred for the orthorhombic ($Pna2_1$-C and $Pnma$-G) ones. A more exact estimate can easily be performed for $Pnma$-G, as we found that in this case the most relevant secondary modes are clearly associated with Bi displacements: By fixing the Bi ions at their high-symmetry positions and relaxing all other structural parameters, we obtained an energy increase of 125 meV/f.u. with respect to the fully relaxed $Pnma$-G structure. Thus, our results show that the energy changes associated with the secondary modes are of the same magnitude as the energy differences between different phases, which implies that these modes play a key role in determining BFO's phase diagram. In particular, the large effects obtained for the orthorhombic phases indicate that their stability depends crucially on occurrence of the AFE patterns associated with Bi's off-centering. We can thus conclude that an effective theory of BFO's structural transitions must account for the effect of these secondary modes.

2. Phenomenological theories

The Devonshire-Landau phenomenological approach to phase transitions in bulk ferroelectrics,[41,42] and its extension to epitaxially constrained films,[43,44] constitutes the simplest, yet powerful, theory that one might try to use to model BFO. Working out such a theory for BFO—i.e., determining the simplest possible Landau potential and temperature dependence of the parameters—constitutes a great challenge that, as far as we know, remains to be tackled. In the following we discuss what our results imply as regards the Landau theory of BFO.

In order to describe all the known phases of this compound, the corresponding Landau potential should be written in terms of a three-dimensional FE polarization **P** (which would correspond to the atomic distortions discussed in Sec. IV B 1), as well as two AFD order parameters associated, respectively, with in-phase and antiphase O_6-octahedra rotations. The cross terms between these three three-dimensional primary order parameters, and the additional terms that will appear if a nonzero epitaxial strain is considered, should allow us to reproduce the intricate energy landscape of BFO and its low-symmetry minima.

Indeed, in cases with several order parameters, it is possible to obtain stable low-symmetry phases from low-order Landau potentials. Imagine, for example, a FE perovskite that develops a polarization along the [1,1,1] direction as well as an in-phase O_6 rotation around the [0,0,1] axis. Such instabilities can be described with a Landau potential truncated at fourth order in both the FE and AFD order parameters. The resulting phase would have a monoclinic Pc (M_A) symmetry, exactly like the Pc-C structure of Table I. Hence, according to this example, it might be possible to describe all BFO's phases with a low-order Landau theory.

However, our results show that the Landau theory for BFO would be significantly more complicated, especially in what regards the relative stability of the large-(c/a) phases. To illustrate this point, let us consider a simplified version of BFO in which only FE distortions and cell strains are allowed, and try to determine the order of the Landau potential $F(\mathbf{P})$ required to describe ferroelectricity in such a system.

In a landmark article, Vanderbilt and Cohen[17] analyzed the form of the Landau potential needed to describe low-symmetry phases in FE perovskites. In essence, they showed that a potential $F(\mathbf{P})$ can present tetragonal or rhombohedral minima if expanded up to fourth order in **P**; the occurrence of orthorhombic minima requires a sixth-order theory, and one needs to go up eighth order to have minima of monoclinic symmetry. This work was essential to understand which Landau potentials are needed to describe the monoclinic phases that were being found at the time in perovskite solid solutions such as $PbZr_{1-x}Ti_xO_3$ (M_A type)[20] and $PbZn_{1/3}Nb_{2/3}O_3$-$PbTiO_3$ (M_C type).[21] The energy landscape associated with an eighth-order potential with a monoclinic M_A minimum is sketched in Fig. 6(a), following the convenient representation scheme introduced in Ref. 17.

We simulated our simplified (FE-only) version of BFO by forcing the material to have a five-atom unit cell in which only polar (Γ_4^-) distortions and cell strains are allowed. (Of course, this cell was appropriately doubled to capture the G- and C-AFM spin arrangements.) If we impose such a constraint to the phases in Table I, we immediately recover the symmetries that were broken by the AFD modes: The Pc-C and Cc-C phases reduce to a single monoclinic M_A structure with space group Cm-C; the Cm-C phase changes to a monoclinic M_C with Pm-C symmetry; $R3c$-G gives us a $R3m$-G phase analogous to BaTiO$_3$'s ground state, etc. We can then consider two additional phases—namely, the supertetragonal $P4mm$-C and orthorhombic $Amm2$-G listed in Table I— to sketch the energy landscape of Fig. 6(b). [To plot Fig. 6(b), the structural stability against Γ-like distortions of the T and M phases was explicitly checked. We have divided the diagram into two sectors to emphasize that the distortions connecting the supertetragonal phases with the rhombohedral and orthorhombic structures are very large.]
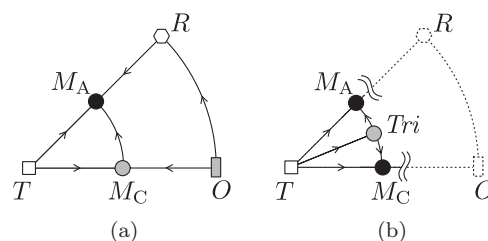

FIG. 6. Energy landscape diagrams as introduced in Ref. 17. Filled, open, and shaded symbols correspond to minima, maxima, and saddle points of the energy, respectively. The T, R, O, and M labels denote phases with exact tetragonal, rhombohedral, orthorhombic, and monoclinic symmetries, respectively. (a) Simplest scenario that gives raise to a monoclinic M_A minimum (Ref. 17). (b) Simplest scenario that gives raise to simultaneous M_A and M_C minima; our discussion focuses on the left part of this diagram (see text).
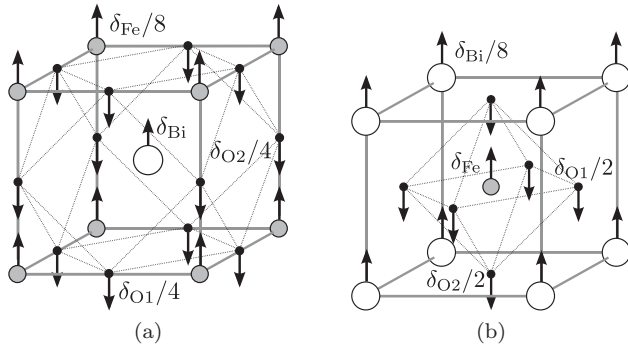
FIG. 7. Examples of local polar modes that can be used as variables of an effective Hamiltonian for BFO. (a) Centered at the Bi atom. (b) Centered at the Fe atom. The quantities δ_I identify displacements of the corresponding I atom in the soft FE mode of the system; they should be divided by a factor that takes into account how many cells share atom I. For BFO we obtained $\delta_{Bi} = 0.80$, $\delta_{Fe} = 0.06$, $\delta_{O1} = -0.42$, and $\delta_{O2} = -0.04$.

The most notable feature of this energy diagram is that it presents two inequivalent monoclinic minima, as opposed to only one as in Fig. 6(a). Further, if we follow the lowest-energy path connecting the M_A and M_C minima through triclinic structures, we will necessarily cross either a saddle point [case depicted in Fig. 6(b)] or a maximum. According to the analysis of Ref. 17, the existence of a triclinic saddle point requires a Landau potential of 10th order, while a 12th-order theory is needed to have a triclinic maximum. Note that Landau potentials of such a high order are unheard of among FE perovskites, even if complex solid solutions are considered. Amusingly, in their paper[17] Vanderbilt and Cohen justified the interest of discussing theories of very high order by writing that "the discovery (or synthesis) of a material having such a behavior may be challenging, but is by no means impossible." Our analysis shows that BFO (even a simplified version of it) is such a material.[45]

3. Atomistic theories

Effective theories of the interatomic interactions in ferroelectric perovskites, with parameters computed from first-principles, were introduced in the early 1990s by Rabe and Vanderbilt.[46] Ever since, these so-called *effective Hamiltonians* have made it possible to perform statistical simulations of increasingly complex materials, from crystalline BaTiO$_3$ (Ref. 46) to disordered PbZr$_{1-x}$Ti$_x$O$_3$,[47] successfully reproducing temperature-driven phase transitions, response properties, etc. More recently, an effective Hamiltonian for BFO has been derived by Kornev *et al.*,[37] who thus extended the approach to incorporate magnetostructural interactions in the model. Such a ground-breaking development has led to great physical insight into BFO's ferroelectric and magnetoelectric properties,[37,48] as well as into the material's behavior under applied electric[49] and magnetic[50] fields. On the other hand, in view of recent experimental results, we now know that some of the model predictions (e.g., the occurrence of a $I4/mcm$ phase at high temperature) are questionable. In the following we briefly summarize what our results teach us about how to construct an accurate effective Hamiltonian for

BFO, extracting the corresponding conclusions as regards the theory of Kornev *et al.*

The first step of the classic approach to constructing effective Hamiltonians consists in identifying the relevant *local* distortions that must be retained in the model, so that we can use a coarse-grained representation of the atoms in the unit cell of our compound. In the case of BFO, there are clearly two local distortions that need to be considered: (1) a polar displacement pattern compatible with the FE (Γ_4^-) soft mode of Fig. 3(a), and (2) the rotation of individual O$_6$ octahedra around an arbitrary axis, whose in-phase (M_3^+) and antiphase (R_4^+) repetitions throughout the crystal reproduce the relevant AFD modes. As shown in Sec. IV B 1, it is enough to consider one local polar mode to reproduce the FE distortion of the $R3c$-G ground state and large-(c/a) phases, which allows us to work with a relatively simple model. A first-principles effective Hamiltonian considering these two types of local variables was first constructed to study SrTiO$_3$,[34] and this was also the starting point of the work of Kornev *et al.* for BFO.

In Sec. IV B 1 we demonstrated the importance of the secondary distortions in determining the relative stability of BFO's phases. The most relevant secondary modes are clearly the Bi-related AFE patterns that occur in the $Pnma$-G and $Pna2_1$-C phases. Fortunately, it is possible to incorporate such effects in an effective Hamiltonian without extending or complicating the model: We can choose the above-mentioned local polar modes to be centered at the Bi atoms, as sketched in Fig. 7(a), so that (i) their homogeneous repetition throughout the crystal reproduces the FE soft mode of Fig. 3(a) and (ii) the zone-boundary modulations reproduce approximately the most relevant AFE distortions of the Bi atoms. Note that, alternatively, one could think of using local polar modes centered at the Fe atoms [see Fig. 7(b)]. However, while this option is valid to reproduce BFO's FE distortions, it fails to capture Bi's AFE patterns (a zone-boundary modulation of the Fe-centered modes results in null Bi displacements).[51] Consequently, an effective model based on Fe-centered modes will put a considerable energy penalty on the $Pnma$-G and similar phases. Such was the approach adopted by Kornev *et al.*, which may explain their prediction that a $I4/mcm$ structure, and not $Pnma$, occurs in the phase diagram of bulk BFO.

As regards the rest of the (less important) secondary modes, it might be possible to incorporate their effect by suitably *renormalizing* the Hamiltonian parameters. To make this idea more precise, let us denote by $\boldsymbol{u}$ ($\boldsymbol{v}$) the distortions that will (will not) be explicitly considered in the model. The usual effective Hamiltonians $H_{\mathrm{eff}}(\boldsymbol{u})$, which work well for materials like BaTiO$_3$ in which secondary distortions are clearly not critical, can be formally defined as

$$H_{\mathrm{eff}}(\boldsymbol{u}) \approx E(\boldsymbol{u},\boldsymbol{v})|_{v=0}, \tag{1}$$

where $E(\boldsymbol{u},\boldsymbol{v})$ is the first-principles energy of an arbitrary configuration of the compound. In contrast, we could define an effective Hamiltonian $\tilde{H}_{\mathrm{eff}}(\boldsymbol{u})$ designed to account for the effect of secondary distortions as

$$\tilde{H}_{\mathrm{eff}}(\boldsymbol{u}) \approx \min_{\boldsymbol{v}} E(\boldsymbol{u},\boldsymbol{v}). \tag{2}$$

Such a refined approach should improve the accuracy of the models in all cases, and it might prove critical to obtain

correct results for compounds as challenging as BFO. The implementation of these ideas remains for future work.

C. The role of bismuth

The Bi cations play a key role in BFO's structural transitions. This can be predicted already from very simple steric arguments: In BiMO_3 perovskites, where M is a first-row transition metal, the lattice parameter is essentially determined by the ionic radii of the metal and oxygen ions. This situation, which corresponds to a small value of the so-called *tolerance factor*,[52] tends to result in either the off-centering of the Bi^{3+} cation or the occurrence of AFD modes, both of which imply the shortening of some Bi-O bonds.[53] This is exactly what is commonly observed in BiMO_3 crystals, and the main reason why some of these compounds make it possible to combine ferroelectricity (related to Bi's off-centering) and magnetism (associated with the transition metals) at high temperatures.

Beyond its relatively small size, Bi^{3+} presents an electronic configuration $(6s^2 p^0)$ that allows for orbital rearrangements suitable to form very directional bonds with neighboring oxygen atoms. Such Bi-O bonds tend to result in a *lone pair* on the nonbonding side, exactly as found in BFO's $R3c$-G phase.[38] This can be readily visualized in an electron-localization-function[54] (ELF) analysis of the computed electronic structure: As shown in Fig. 8(a), there is a distinct nonbonding localization domain on the side of Bi that is opposite to the three neighboring O atoms, which is the signature of a lone pair.[55,56] The occurrence of such a lone pair was discussed at length by Ravindran *et al.*[38] on the basis of first-principles calculations similar to ours; our results for BFO's $R3c$-G phase [Figs. 8(a) and 9(a)] essentially reproduce their study.[57]

We computed the ELF maps for the other BFO phases found in this work. Figure 8 shows the results for two representative cases: Cc-C and $Pnma$-G. It is immediate clear that a lone pair forms in the supertetragonal Cc-C phase, as might have been expected from Bi's large off-centering and the anisotropic spatial distribution of its neighboring oxygens. The case of $Pnma$-G is quite different, though: As shown in Fig. 8(c), in this phase the Bi cations have four neighboring oxygens that form a rather regular BiO_4 tetrahedron. The corresponding ELF plots show a very isotropic localization domain around Bi. There is no clear lone-pair formation in this case; further, such a localization domain is not typical of bonding electrons, as evidenced by the slightly smaller ELF values along the directions of the Bi-O bonds. Hence, it might be more appropriate to interpret this result as corresponding to a semicore-like case. Interestingly, the partial density of states results shown in Fig. 9 indicate that these three phases are very similar as regards orbital occupation, even if they clearly differ in terms of Bi-O bonding and lone-pair occurrence. Hence, our results illustrate Bi's electronic flexibility and its ability to form different *coordination complexes* with the neighboring oxygens.

These chemical effects are clearly the driving force for the structural transitions in BFO. Note that *all* the BFO phases discussed here, either ferroelectric or paraelectric, have an energy that is lower than that of the cubic structure by more than 800 meV/f.u. (see Table I). In contrast, the cubic and polar phases differ by about 15 meV/f.u. in the case of the prototype ferroelectric $BaTiO_3$, where the Coulomb
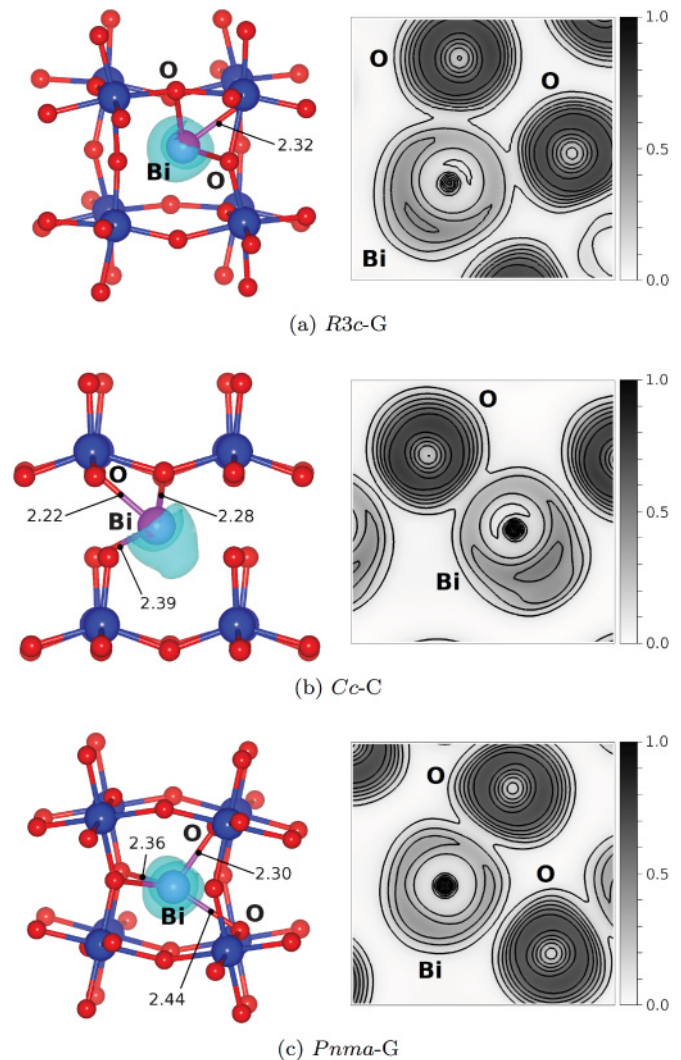

(a) $R3c$-G

(b) Cc-C

(c) $Pnma$-G

FIG. 8. (Color online) Electronic-localization-function (ELF) maps computed for the $R3c$-G, Cc-C, and $Pnma$-G phases. The figures on the left show the isosurface for an ELF value of 0.3 superimposed onto the atomic structure; on the right we show the ELF contour plots in the planes defined by the labeled ions. We also indicate the shortest Bi-O distances (in angstroms) as obtained from PBEsol+U calculations.

dipole-dipole interactions are known to be the driving force for the FE instability.[58] Noting that BFO and $BaTiO_3$ are rather similar as regards the magnitude of the dipole-dipole forces,[59] we can conclude that such an enormous difference in the strength of the structural instabilities must be associated with the dominant role of the Bi-O chemistry in BFO. Then, the relative stability of BFO's low-energy phases is probably determined by factors that involve smaller energy differences, such as subtle competitions between different Bi-O bonding mechanisms, the buildup of dipole-dipole interactions in the FE phases, etc. Analyzing these issues in detail falls beyond the scope of the present work. We hope our findings will stimulate further theoretical studies of the chemical bond in these phases, so that the factors controlling the occurrence of AFD and/or FE distortions (especially the supertetragonal ones) can be elucidated.
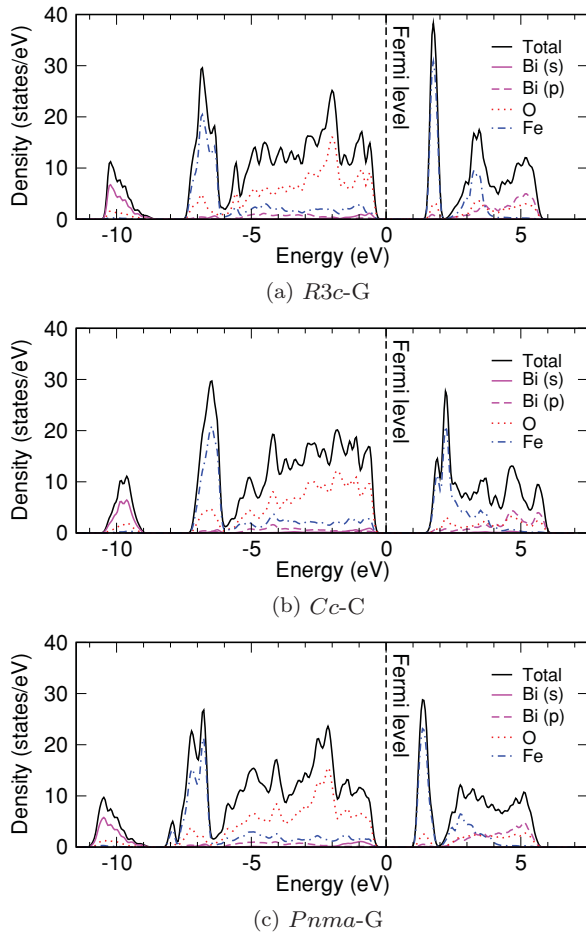
FIG. 9. (Color online) Electronic density of states for the *R3c*-G, *Cc*-C, and *Pnma*-G phases, as obtained from PBEsol+*U* calculations. Note that, in these AFM phases, the results for the spin-up and spin-down channels are identical.

Let us conclude by noting that our results for BFO—with most phases being dominated by either AFD or FE distortions—are clearly reminiscent of the competition between AFD and FE instabilities that is well known to occur in many perovskite oxides. Such a competition has been studied in detail in SrTiO₃,[34] and is one of the factors responsible for the rich phase diagram of materials like PbZr$_{1-x}$Ti$_x$O₃.[60] Interestingly, BFO is peculiar inasmuch its FE soft mode is dominated by the *A*-site cation, whereas ferroelectricity in SrTiO₃ is driven by the *B*-site transition metal and PbZr$_{1-x}$Ti$_x$O₃ is an intermediate case. Hence, BFO may constitute an additional model system for the investigation of competing-instability phenomena in perovskite oxides.

V. SUMMARY AND CONCLUSIONS

We have used first-principles methods to perform a systematic search for potentially stable phases of multiferroic BiFeO₃. We worked with a 40-atom super-cell (i.e., a $2 \times 2 \times 2$ repetition of the cubic perovskite cell) that is compatible with the atomic distortions that are most common among transition-metal perovskite oxides, namely, ferroelectric, antiferroelectric, and anti-ferrodistortive. We obtained plenty of distinct low-energy phases of the compound; here we have restricted

the discussion to the most stable ones. Many of the minima obtained present complex structural distortions and very low symmetry (e.g., monoclinic M_A and M_C space groups) while preserving a relatively small unit cell. As far as we know, this is quite unique among perovskite oxides, as the monoclinic structures reported so far are associated with complex solid solutions (e.g., PbZr$_{1-x}$Ti$_x$O₃ or PbZn$_{1/3}$Nb$_{2/3}$O₃-PbTiO₃), present large unit cells (e.g., BiMnO₃ and BiScO₃), or are obtained under special conditions (e.g., thin films subject to appropriate epitaxial strains or bulk compounds under external electric fields). In contrast, our study shows that bulk BiFeO₃ presents *per se* a collection of *simple* low-symmetry minima of the energy.

Our findings have a number of important implications for the research on BiFeO₃ and related materials. Maybe the most general and interesting one stems from the demonstration that BFO can form plenty of (meta)stable structural phases, which suggests that recent puzzling observations—ranging from possible structural transitions at low temperatures[61] to surface-specific atomic structures[62] and strain-induced new phases[5,22]—may just be reflecting BFO's intrinsic structural richness. Additionally, our results will provide useful information to the experimental workers exploring the possibility of obtaining large functional (piezoelectric, magnetoelectric) effects in BiFeO₃ films grown on strongly compressive substrates: We have shown that there are plenty of phases—all with large polarizations and *c/a* aspect ratios—that can be realized in such conditions, including possibilities with monoclinic and orthorhombic symmetries. Our results also provide insights concerning the relative importance of the various structural distortions that can occur in BiFeO₃, stressing the key role that the so-called *secondary modes* play in determining the relative stability of the observed phases.

Our work also has implications for theoretical studies of BiFeO₃. First, we present a critical comparison of the various DFT schemes most commonly employed to study BiFeO₃ and related compounds, and discuss the existing difficulties in quantifying the relative phase stability. Second, we draw important conclusions as regards the effective modeling of structural phase transitions in BiFeO₃, in connection with both Landau-type and atomistic theories. Our analysis shows that BiFeO₃ is rather unusual, and that its modeling needs to address issues—ranging from the work with high-order Landau potentials to the accurate treatment of secondary distortions—that are unheard of in the work with *classic* materials such as BaTiO₃, PbZr$_{1-x}$Ti$_x$O₃, or even relaxor ferroelectrics. Finally, our results provide quantitative evidence for the dominant role that the Bi-O bond formation plays in BiFeO₃'s structural instabilities. Further, our analysis suggests that some of the phases discussed here do not exhibit the "lone-pair mechanism" usually invoked to explain the Bi-O directional bonds in BiFeO₃. We take this as a further illustration of Bi's ability to form diverse, competitive in energy, bonding complexes with its neighboring oxygens.

In conclusion, we have used first-principles simulation methods to illustrate, quantify, and analyze in some detail the structural richness of BiFeO₃, the most relevant representative of the family of Bi-based transition-metal perovskite oxides. Our simulations have revealed a variety of unusual effects,

some of which have important implications for current experimental and theoretical research on this material. We thus hope this work will help clarify and further stimulate research on these ever-surprising compounds.

---

[1] G. Catalan and J. F. Scott, Adv. Mater. **21**, 2463 (2009).

[2] J. Seidel *et al.*, Nat. Mater. **8**, 229 (2009).

[3] H. Béa *et al.*, Phys. Rev. Lett. **102**, 217603 (2009).

[4] I. C. Infante *et al.*, Phys. Rev. Lett. **105**, 057601 (2010).

[5] R. J. Zeches *et al.*, Science **326**, 977 (2009).

[6] J. C. Wojdeł and J. Íñiguez, Phys. Rev. Lett. **105**, 037208 (2010).

[7] M. Azuma *et al.*, Jpn. J. Appl. Phys. **47**, 7579 (2008).

[8] D. Kan *et al.*, Adv. Funct. Mater. **20**, 1108 (2010).

[9] J. P. Perdew and A. Zunger, Phys. Rev. B **23**, 5048 (1981); D. M. Ceperley and B. J. Alder, Phys. Rev. Lett. **45**, 566 (1980).

[10] J. P. Perdew, K. Burke, and M. Ernzerhof, Phys. Rev. Lett. **77**, 3865 (1996).

[11] J. P. Perdew, A. Ruzsinszky, G. I. Csonka, O. A. Vydrov, G. E. Scuseria, L. A. Constantin, X. Zhou, and K. Burke, Phys. Rev. Lett. **100**, 136406 (2008).

[12] G. Kresse and J. Furthmuller, Phys. Rev. B **54**, 11169 (1996); G. Kresse and D. Joubert, *ibid.* **59**, 1758 (1999).

[13] S. L. Dudarev, G. A. Botton, S. Y. Savrasov, C. J. Humphreys, and A. P. Sutton, Phys. Rev. B **57**, 1505 (1998). We determined the value of $U = 4$ eV by requesting the computed magnetic interactions to be in quantitative agreement with those obtained from calculations with hybrid functionals. Note that $U \approx 4$ eV has become a frequent choice in first-principles studies of BFO, as it leads to qualitatively and semiquantitatively correct results for all the properties investigated so far.

[14] P. E. Blochl, Phys. Rev. B **50**, 17953 (1994); G. Kresse and D. Joubert, *ibid.* **59**, 1758 (1999).

[15] A. M. Glazer, Acta Crystallogr., Sect. B **28**, 3384 (1972).

[16] The reported P values were obtained as half of the polarization change between the "$+P$" and "$-P$" states. For the T phases, special care was needed to identify an insulating path connecting such polar states, as we found that centrosymmetric structures with a large-(c/a) cell tend to be metallic. Hence, our paths for the T phases go through a small-(c/a) centrosymmetric structure.

[17] D. Vanderbilt and M. H. Cohen, Phys. Rev. B **63**, 094108 (2001).

[18] A. J. Hatt, N. A. Spaldin, and C. Ederer, Phys. Rev. B **81**, 054109 (2010).

[19] Given the minute energy differences associated with such symmetry breakings, one can expect quantum lattice-dynamical effects to play a role in determining which phase is most stable. Indeed, detailed first-principles studies have shown that such zero-point effects, which will typically favor high-symmetry phases, may have a great impact in the phase diagram of perovskite oxides, as, e.g., in *quantum paraelectric* $SrTiO_3$ [W. Zhong and D. Vanderbilt, Phys. Rev. B **53**, 5047 (1996)] and even strong ferroelectric $BaTiO_3$ [J. Íñiguez and D. Vanderbilt, Phys. Rev. Lett. **89**, 115503 (2002)].

[20] B. Noheda *et al.*, Appl. Phys. Lett. **74**, 2059 (1999).

[21] B. Noheda, D. E. Cox, G. Shirane, S.-E. Park, L. E. Cross, and Z. Zhong, Phys. Rev. Lett. **86**, 3891 (2001).

[22] R. Haumont, P. Bouvier, A. Pashkin, K. Rabia, S. Frank, B. Dkhil, W. A. Crichton, C. A. Kuntscher, and J. Kreisel, Phys. Rev. B **79**, 184110 (2009).

[23] D. I. Bilc, R. Orlando, R. Shaltaf, G. M. Rignanese, J. Iniguez, and P. Ghosez, Phys. Rev. B **77**, 165107 (2008).

[24] We ran fixed-volume structural relaxations of the relevant phases in the range shown in Fig. 1.

[25] O. E. González-Vázquez, J. C. Wojdeł, O. Diéguez, and J. Íñiguez (unpublished).

[26] We ran epitaxially constrained structural relaxations of the relevant phases in the range shown in Fig. 5. We forced the 40-atom cell of Fig. 1 to be square in the (001) plane.

[27] C. J. M. Daumont, S. Farokhipoor, A. Ferri, J. C. Wojdeł, J. Íñiguez, B. J. Kooi, and B. Noheda, Phys. Rev. B **81**, 144115 (2010).

[28] O. Diéguez and J. Íñiguez (unpublished).

[29] Z. Wu and R. E. Cohen, Phys. Rev. B **73**, 235116 (2006).

[30] Z. Chen *et al.*, Appl. Phys. Lett. **96**, 252903 (2010).

[31] Z. Chen *et al.*, Adv. Funct. Mater. **21**, 133 (2011).

[32] J. H. Nam, H. S. Kim, A. J. Hatt, N. A. Spaldin, and H. M. Christen, e-print arXiv:1010.0254.

[33] At finite temperatures, the relative phase stability will be determined by effects (e.g., vibrational entropy or thermal expansion) not considered here. Additionally, the transition temperatures may be strongly conditioned by the presence of competing instabilities (Ref. 34) whose correct treatment may require a full statistical calculation.

[34] W. Zhong and D. Vanderbilt, Phys. Rev. Lett. **74**, 2587 (1995).

[35] R. Palai, R. S. Katiyar, H. Schmid, P. Tissot, S. J. Clark, J. Robertson, S. A. T. Redfern, G. Catalan, and J. F. Scott, Phys. Rev. B **77**, 014110 (2008).

[36] D. C. Arnold *et al.*, Adv. Funct. Mater. **20**, 2116 (2010).

[37] I. A. Kornev, S. Lisenkov, R. Haumont, B. Dkhil, and L. Bellaiche, Phys. Rev. Lett. **99**, 227602 (2007).

[38] P. Ravindran, R. Vidya, A. Kjekshus, H. Fjellvag, and O. Eriksson, Phys. Rev. B **74**, 224412 (2006).

[39] R. D. King-Smith and D. Vanderbilt, Phys. Rev. B **49**, 5828 (1994).

[40] Strictly speaking, the cell strain associated with the large-(c/a) ratios of our T phases is a secondary order parameter. However, we recognize its obvious importance and do not consider it in this discussion.

[41] F. Devonshire, Philos. Mag. **40**, 1040 (1949); **42**, 1065 (1951); Adv. Phys. **3**, 85 (1954).

[42]J. Íñiguez, S. Ivantchev, J. M. Pérez-Mato, and A. García, Phys. Rev. B **63**, 144103 (2001).

[43]N. A. Pertsev, A. G. Zembilgotov, and A. K. Tagantsev, Phys. Rev. Lett. **80**, 1988 (1998).

[44]O. Dieguez, S. Tinte, A. Antons, C. Bungaro, J. B. Neaton, K. M. Rabe, and D. Vanderbilt, Phys. Rev. B **69**, 212101 (2004).

[45]As our discussion suggests, it might be possible to construct a lower-order Landau potential, and correctly account for all the low-symmetry minima, if additional degrees of freedom are explicitly considered in the theory. In the case of our simplified FE-only version of BFO, such additional degrees of freedom should be the cell strains.

[46]W. Zhong, D. Vanderbilt, and K. M. Rabe, Phys. Rev. Lett. **73**, 1861 (1994).

[47]L. Bellaiche, A. García, and D. Vanderbilt, Phys. Rev. Lett. **84**, 5427 (2000).

[48]D. Albrecht, S. Lisenkov, W. Ren, D. Rahmedov, I. A. Kornev, and L. Bellaiche, Phys. Rev. B **81**, 140401 (2010).

[49]S. Lisenkov, D. Rahmedov, and L. Bellaiche, Phys. Rev. Lett. **103**, 047204 (2009).

[50]S. Lisenkov, I. A. Kornev, and L. Bellaiche, Phys. Rev. B **79**, 012101 (2009).

[51]The details associated with the choice of local modes for effective Hamiltonians of FE perovskites, and the corresponding symmetry analysis, are discussed at length in K. M. Rabe and U. V. Waghmare, Phys. Rev. B **52**, 13236 (1995).

[52]J. Íñiguez, D. Vanderbilt, and L. Bellaiche, Phys. Rev. B **67**, 224107 (2003).

[53]Revealingly, the ionic radius of Bi^{3+} for a XII oxygen coordination, such as the one of the *A* site in the cubic perovskite structure, does not appear in the well-known tables compiled by Shannon [R. D. Shannon, Acta Crystallogr., Sect. A **32**, 751 (1976)].

[54]B. Silvi and A. Savin, Nature (London) **371**, 683 (1994).

[55]A. Savin, R. Nesper, S. Wengert, and T. F. Fässler, Angew. Chem. Int. Ed. **36**, 1808 (1997).

[56]D. B. Chesnut, J. Phys. Chem. A **104**, 11644 (2000).

[57]As compared with the results of Ref. 38, we obtained relatively small ELF values in the lone-pair region. Such differences are most likely related to some technicalities of the calculations, in particular to the use of different numbers of valence electrons.

[58]P. Ghosez, E. Cockayne, U. V. Waghmare, and K. M. Rabe, Phys. Rev. B **60**, 836 (1999).

[59]The magnitude of the dipole-dipole interactions is essentially controlled by the Born effective charges Z^* (which quantify the electric polarization that appears as a consequence of an atomic displacement) and the electronic dielectric constant ϵ_∞ (which quantifies the system's ability to screen electrostatic interactions). All the atoms in $BiFeO_3$ and $BaTiO_3$ present large Z^* values that exceed the nominal ionization charges by a factor of 2 at most; we obtained $\epsilon_\infty \approx 7$ for $BaTiO_3$ and $\epsilon_\infty \approx 10$ for $BiFeO_3$. Such deviations cannot account for the large difference in the energetics of the structural instabilities of these compounds.

[60]I. A. Kornev, L. Bellaiche, P.-E. Janolin, B. Dkhil, and E. Suard, Phys. Rev. Lett. **97**, 157601 (2006).

[61]S. A. T. Redfern, C. Wang, J. W. Hong, G. Catalan, and J. F. Scott, J. Phys. Condens. Matter **20**, 452205 (2008); J. Herrero-Albillos *et al.*, *ibid.* **22**, 256001 (2010).

[62]X. Martí *et al.*, e-print arXiv:1012.2306.

[63]K. Momma and F. Izumi, J. Appl. Crystallogr. **41**, 653 (2008).

[64][http://www.jmol.org/].

[65]M. I. Aroyo *et al.*, Z. Kristallogr. **221**, 15 (2006); M. I. Aroyo, A. Kirov, C. Capillas, J. M. Perez-Mato, and H. Wondratschek, Acta Crystallogr., Sect. A **62**, 115 (2006).

[66]B. J. Campbell, H. T. Stokes, D. E. Tanner, and D. M. Hatch, J. Appl. Crystallogr. **39**, 607 (2006).